Applied Energy 99 (2012) 379–385

Contents lists available at SciVerse ScienceDirect

Applied Energy

journal homepage: www.elsevier.com/locate/apenergy

A 1 kW_e thermoelectric stack for geothermal power generation – Modeling and geometrical optimization

C. Suter [a], Z.R. Jovanovic [a], A. Steinfeld [a,b,*]

[a] Department of Mechanical and Process Engineering, ETH Zurich, 8092 Zurich, Switzerland
[b] Solar Technology Laboratory, Paul Scherrer Institute, 5232 Villigen, Switzerland

HIGHLIGHTS

- A 1 kW_e thermoelectric stack is considered for geothermal heat conversion.
- It comprises an array of Bi–Te modules between counter-flow water heat exchangers.
- A coupled conduction–convection heat transfer model was formulated.
- Optimization is accomplished for either maximum efficiency (η) or minimum volume (V).
- For hot water inlet/outlet temperatures (413 K/393 K), $\eta = 4.2\%$ and $V = 0.0021$ m^3.

ARTICLE INFO

Article history:
Received 27 January 2012
Received in revised form 8 May 2012
Accepted 10 May 2012
Available online 28 June 2012

Keywords:
Thermoelectric
Stack
Geothermal
Modeling
Optimization

ABSTRACT

A thermoelectric stack comprising an array of Bi–Te based thermoelectric converter (TEC) modules is considered for geothermal heat conversion. Each TEC module consists of 127 $(Bi_{0.2}Sb_{0.8})_2Te_3/Bi_2(Te_{0.96}Se_{0.04})_3$ p/n-type thermoelement pairs, fastened by 30×30 mm^2 Al_2O_3 plates. The thermoelement pairs have leg cross-section of 1.05×1.05 mm^2, a figure-of-merit equal to 1, and a theoretical heat-to-electricity conversion efficiency of ~5% when the module is operated at a temperature difference of 200 K. A temperature gradient across the thermoelement legs within an array is imposed via a Cu parallel-plate heat exchanger adhering to the Al_2O_3 plates and operating hot and cold water in counter-flow channel configuration. A heat transfer model coupling conduction through the thermoelement legs with convection to and from the Al_2O_3 plates is formulated to investigate the performance of the stack as function of the following parameters: hot water inlet and outlet temperatures (313–413 K and 303–393 K, respectively), stack length (300–1500 mm), thermoelement leg length (0.5–4 mm) and hot/cold channel heights (0.2–2 mm). The open-circuit voltages resulting from the temperature differences are within 3% mean relative error of those resulting from temperature differences computed via CFD. The heat transfer model is then applied to optimize a 1 kW_e stack with hot water inlet and outlet temperatures of 413 K and 393 K, respectively, for either a maximum heat-to-electricity efficiency of 4.2% or for a minimum volume of 0.0021 m^3.

1. Introduction

In 2010, the globally installed thermal power of geothermal low-temperature heat (<150 °C at a borehole depth of <4 km) was 50.6 MW_e with an annual growth rate of 12.3% [1–3]. Geothermal low-temperature heat has been commonly used for district heating or driving heat pumps. As of recently, it has also been considered for electricity generation by thermoelectric converters (TEC) [4–6].

A TEC module comprises p-type and n-type semiconductor thermoelement legs fastened between two ceramic hot/cold plates and connected in parallel thermally and in series electrically [7–9]. The temperature gradient across the legs induces a voltage due to the Seebeck effect [10]. The TEC performance is characterized by its figure-of-merit (ZT) which is a measure of the heat-to-electricity efficiency: the higher the ZT, the higher the heat-to-electricity efficiency is, approaching the Carnot efficiency for $ZT \to \infty$. A state-of-the-art BiTe based module having $ZT = 1$ and operating at 200 K temperature difference reaches the theoretical maximum efficiency of 5% [11].

Thermoelectric stacks comprising arrays of TEC modules adhering to parallel-, counter- and cross-flow water heat exchangers

* Corresponding author at: Department of Mechanical and Process Engineering, ETH Zurich, 8092 Zurich, Switzerland.
E-mail address: aldo.steinfeld@ethz.ch (A. Steinfeld).

0306-2619/$ - see front matter © 2012 Elsevier Ltd. All rights reserved.
http://dx.doi.org/10.1016/j.apenergy.2012.05.033

Nomenclature

A	surface (m^2)
B	domain boundary (m^2)
c_p	heat capacity ($J\,kg^{-1}\,K^{-1}$)
f	friction factor
h	heat transfer coefficient ($W\,m^{-2}\,K^{-1}$)
H	height (m)
j	electric current density ($A\,m^{-2}$)
J	electric current (A)
l	leg length (m)
L	stack length (m)
m	water mass flow ($kg\,s^{-1}$)
M	number of thermoelement legs
n	normal vector
N	number of modules
P	electric power (W)
q	heat flux ($W\,m^{-2}$)
Q	heat transferred (W)
R	electrical resistance (Ω)
R^2	coefficient of determination
S	Seebeck coefficient ($V\,K^{-1}$)
t	thickness (m)
T	temperature (K)
u	velocity ($m\,s^{-1}$)
U	voltage (V)
V	volume (m^3)
$\dot{V}$	volume flow ($m^3\,s^{-1}$)
W	width (m)

Greek letters

α,β	correction factors
γ	iteration step
ε	error
κ	thermal conductivity ($W\,m^{-1}\,K^{-1}$)
η	heat-to-electricity efficiency
ρ	density ($kg\,m^{-3}$)
ρ	electrical resistivity ($\Omega\,m$)
$\hat{\rho}$	electrical contact resistivity ($\Omega\,m^2$)
σ	power density ($W\,m^{-3}$)
θ	pressure (Pa)

Subscripts

c	cold
conv	convection
e	electric
h	hot
i	finite volume index
leg	thermoelement leg
m	middle
OC	open-circuit
seg	stack segment
w	water

Abbreviations

CFD	computational fluid dynamics
ZT	figure-of-merit
TEC	thermoelectric converter

have been previously analyzed [5,12–16]. The effect of the dimensions of the TEC modules and flow channels on the conversion efficiency has been examined for a stack with counter-flow configuration [5,16]. This paper expands on previous studies by including into the analysis the effect of the geothermal reservoir temperature, i.e., heat transfer fluid inlet temperature, on the performance of a 1 kW_e stack comprising arrays of TEC modules with counter-flow heat exchangers. A heat transfer model coupling conduction through the thermoelement legs with convection to and from the boundary plates is formulated after evaluating the predominant modes of heat transfer. It further accounts for temperature-dependent physical properties and heat transfer coefficients across flow regimes. The model was numerically solved to analyze the heat-to-electricity efficiency η_{stack} and stack volume V_{stack} as a function of a wide hot water inlet and outlet temperature range and geometrical parameters. Optimization of the stack configuration is accomplished for either (a) maximum V_{stack} or (b) minimum η_{stack} (maximum power density).

2. Scheme of thermoelectric stack

The modular stack configuration is schematically shown in Fig. 1. The stack comprises lateral arrays of TEC modules. Each module is represented by a pair of Al_2O_3 plates fastening 127 pairs of p/n-type $(Bi_{0.2}Sb_{0.8})_2Te_3/Bi_2(Te_{0.96}Se_{0.04})_3$ thermoelement legs ($M = 254$) [17]. The surface of the Al_2O_3 plates and the cross section of the thermoelement legs are $A_{plate} = 30 \times 30\,mm^2$ and $A_{leg} = 1.05 \times 1.05\,mm^2$, respectively; the lengths of the stack (L) and the thermoelement legs (l) are allowed to vary as model parameters. A temperature gradient across the thermoelement legs is imposed via a parallel-plate heat exchanger separating the thermoelectric arrays and operating hot and cold water in the counter-flow configuration. The heat exchanger is made of 1 mm thick Cu plates adhering to the 0.5 mm thick Al_2O_3 plates.

3. Heat transfer model

The heat transfer model has been developed for a stack segment outlined by the dashed line in Fig. 1. A more detailed schematic of the segment is shown by Fig. 2 representing it as an array of N_{array} TEC modules having the total length L, the width $W = 30$ mm, and hot and cold water half-channels with thickness t_h and t_c, respectively, resulting in the total height $H = l + t_h + t_c + 2 \cdot t_{plate} + 2 \cdot t_{Cu}$. The following assumptions have been made: (i) heat transfer by radiation and free convection between hot and cold Al_2O_3 plates is neglected as their contribution compared to the total heat transfer has been estimated by CFD to be less than 5% (Appendix A), (ii) the thermal resistances for the heat conduction through the Cu and Al_2O_3 plates is neglected, and (iii) the hot and cold sides of the legs within a module have uniform temperatures. Thus, the heat transfer is considered to occur via: (1) convection between water and the thermoelement legs, and (2) 1D conduction through the thermoelement legs. Furthermore, it is assumed that the hot and cold sides of the legs within a module have uniform temperatures. The model only considers steady-state.

3.1. Governing equations

Heat transfer is formulated for the hot side only due to the complete analogy with the cold side. The general continuous energy conservation equation in integral form for the hot water channel considering heat transport by the water flow and heat convection through walls is given in terms of the hot water temperature $T_{w,h}$, the velocity vector of the water flow $\underline{u}_h$, the normal vector of the channel domain $\underline{n}_h$, the convective heat flux $\underline{q}_{conv,h}$ and the channel domain boundary B by [18]:

$$\int_B \rho_W \cdot c_{p,w} \cdot T_{w,h} \cdot (\underline{u}_h \cdot \underline{n}_h) \cdot dB = -\int_B \underline{q}_{conv,h} \cdot \underline{n}_h \cdot dB \qquad (1)$$

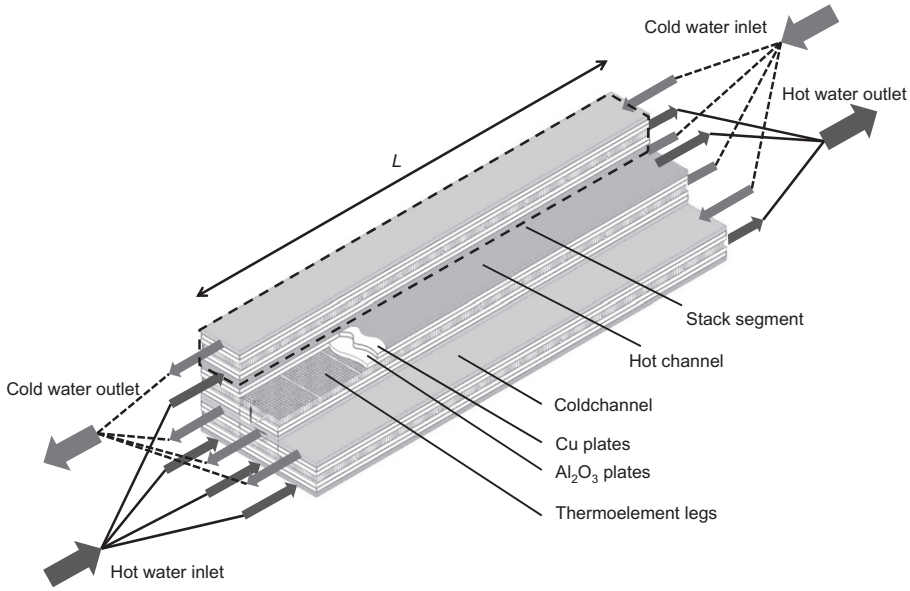

Fig. 1. Schematic of the thermoelectric stack with arrays of TEC modules separated by Cu plate heat exchangers in counter-flow configuration. The dashed line outlines a stack segment for which the heat transfer model has been developed.

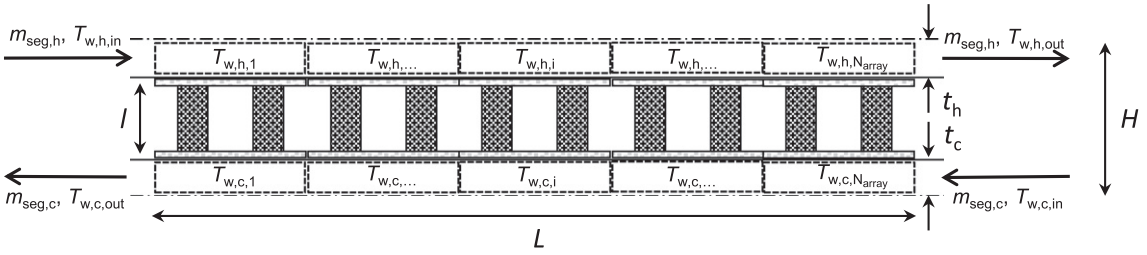

Fig. 2. Schematic of the modeled stack segment: an array of stack length L with N_{array} TEC modules having a leg length l between hot and cold water half-channels of thickness t_h and t_c, respectively, resulting in the height H. The channels are discretized into N_{array} cells (dotted boxes), having the uniform water temperatures $T_{w,h,i}$ and $T_{w,c,i}$ within the cell i, respectively. The dashed–dotted lines indicate symmetry boundaries.

By applying the finite volume method, the hot water channel is discretized into N_{array} rectangular cells (control volumina, see dotted boxes in Fig. 2), having the uniform discrete temperature $T_{w,h,i}$ within a single cell. For the discretization the following relations are used: $m_{seg,h} = \rho_w \cdot u_h \cdot A_{channel}$, $A_{channel} = W \cdot t_h$ and $q_{conv,h} = h_{h,i} \cdot (T_{w,h,i} - T_{leg,h,i})$. Then the discretized equation in the cell i in terms of hot water mass flow $m_{seg,h}$, hot water temperature $T_{w,h,i}$ and hot side leg temperature $T_{leg,h,i}$ yields [19]:

$$c_{p,w,i} \cdot m_{seg,h} \cdot \left(\frac{T_{w,h,i-1} + T_{w,h,i}}{2} - \frac{T_{w,h,i} + T_{w,h,i+1}}{2} \right) = h_{h,i} \cdot A_{plate} \cdot (T_{w,h,i} - T_{leg,h,i}) \quad (2)$$

The convective (hot water)-to-(thermoelement leg) heat transfer coefficients $h_{h,i}$ have been determined from Nusselt correlations for laminar, transitional and turbulent flows between parallel flat plates [20–23]. The continuous energy conservation equation in differential form for the thermoelement legs considering Fourier's heat conduction, Joule heating, and Thomson effect is given in terms of the temperature in the leg T_{leg} and the current density $\underline{j}$ by:

$$\nabla(\kappa_{leg} \cdot \nabla T_{leg}) + \rho_{leg} \cdot \underline{j}^2 - T_{leg} \cdot \frac{dS_{leg}}{dT_{leg}} \cdot \underline{j} \cdot \nabla T_{leg} = 0 \quad (3)$$

where the current density $\underline{j}$ satisfies current conservation $\nabla \underline{j} = 0$ and is given in terms of the voltage U_{leg} and the leg temperature T_{leg} by:

$$\underline{j} = -\frac{1}{\rho_{leg}} \left[\nabla U_{leg} + S_{leg} \cdot \nabla T_{leg} \right] \quad (4)$$

With the assumption of 1D heat conduction in the thermoelement legs, linear dependency of the thermoelectric material properties on temperature and the overall current J, Eq. (3) can be algebraically solved. Thus, the 1D heat conduction at the hot side of a thermoelement leg in the cell i in terms of the hot side leg temperature $T_{leg,h,i}$, the overall current J and the temperature difference across the legs ($\Delta T_{leg,i} = T_{leg,h,i} - T_{leg,c,i}$) reduces to:

$$Q_{leg,h,i} = S_{leg,m,i} \cdot T_{leg,h,i} \cdot J - \alpha_{h,i} \cdot l \cdot \frac{\rho_{leg,m,i}}{A_{leg}} \cdot J^2/2 + \beta_{h,i} \cdot A_{leg} \cdot \frac{\kappa_{leg,m,i}}{l} \cdot \Delta T_{leg,i} \quad (5)$$

where

$$\alpha_{h,i} = \left(1 + \frac{1}{\rho_{leg,m,i}} \cdot \frac{d\rho_{leg,m,i}}{dT_{leg,m,i}} \cdot \frac{\Delta T_{leg,i}}{4} \right) \quad (6)$$

and

$$\beta_{h,i} = \left[1 - \left(\frac{1}{\kappa_{leg,m,i}} \cdot \frac{d\kappa_{leg,m,i}}{dT_{leg,m,i}} \cdot \Delta T_{leg,i} \right)^2 \Big/ 12 \right] \quad (7)$$

are the correction factors accounting for the linear dependency of the material properties on temperature [24]. As aforementioned,

the heat transfer considerations for the cold side are analogous to the ones presented above. Further the electric current is given by:

$$J = U_{\text{array}}/(R_{\text{array}} + R_{\text{contact}} + R_{\text{load}}) \tag{8}$$

The voltage is:

$$U_{\text{array}} = M \cdot \sum_{i=1}^{N_{\text{array}}} S_{\text{leg,m,i}} \cdot \Delta T_{\text{leg,i}} \tag{9}$$

the material resistance:

$$R_{\text{array}} = M \cdot \frac{l}{A_{\text{leg}}} \sum_{i=1}^{N_{\text{array}}} \rho_{\text{leg,m,i}} \tag{10}$$

and the contact resistance:

$$R_{\text{contact}} = 2 \cdot N_{\text{array}} \cdot M \cdot \frac{\hat{\rho}}{A_{\text{leg}}} \tag{11}$$

with the matched load:

$$R_{\text{load}} = R_{\text{contact}} + R_{\text{array}} \tag{12}$$

The power output of the TEC module array is calculated by:

$$P_{\text{array}} = J^2 \cdot R_{\text{load}} \tag{13}$$

and the useful power output of the stack segment is given by:

$$P_{\text{seg}} = P_{\text{array}} - P_{\text{pump}} \tag{14}$$

where the pump work P_{pump} is estimated in terms of the pressure drop in the water channels and the volume flow. The pressure drop in the hot channel – analogously for the cold channel – is estimated in terms of the friction factor f_{h} and the flow velocity u_{h} by:

$$\Delta\Theta_{\text{h}} = f_{\text{h}} \frac{L}{t_{\text{h}}} \left(\frac{1}{2} \cdot \rho_{\text{w}} \cdot u_{\text{h}}^2 \right) \tag{15}$$

The friction factor f_{h} has been determined for laminar, transitional, and turbulent flows between parallel flat plates [20,22]. Then the pumping work in the hot channel (analogously for the cold channel) is calculated in terms of the pressure drop $\Delta\Theta_{\text{h}}$ and the volume flow $\dot{V}_{\text{h}}$ by:

$$P_{\text{pump,h}} = \dot{V}_{\text{h}} \cdot \Delta\Theta_{\text{h}} \tag{16}$$

Evidently, the total pumping work is then $P_{\text{pump}} = P_{\text{pump,h}} + P_{\text{pump,c}}$. Finally, the heat-to-electricity efficiency of the stack segment η_{seg} is defined as the ratio of the electrical power output over the heat delivered to the stack segment:

$$\eta_{\text{seg}} = \frac{P_{\text{seg}}}{m_{\text{seg,h}} \cdot c_{\text{p,w}} \cdot \Delta T_{\text{w,h}}} \tag{17}$$

The volume of the stack segment is given in terms of the stack length L, the stack segment height H, and the stack segment width W by:

$$V_{\text{seg}} = L \cdot H \cdot W \tag{18}$$

The power density of the stack segment is expressed as:

$$\sigma_{\text{seg}} = \frac{P_{\text{seg}}}{V_{\text{seg}}} \tag{19}$$

Finally for the total stack, the magnitudes η_{stack}, V_{stack}, $m_{\text{h,stack}}$ N_{stack}, and σ_{stack} are calculated in terms of the ratio of the power outputs of the stack P_{stack} and stack segment P_{seg} by:

$$\eta_{\text{stack}} = \eta_{\text{seg}},\ V_{\text{stack}} = V_{\text{seg}} \cdot \frac{P_{\text{stack}}}{P_{\text{seg}}},\ m_{\text{h,stack}} = m_{\text{h,seg}} \cdot \frac{P_{\text{stack}}}{P_{\text{seg}}},\ N_{\text{stack}} = N_{\text{array}} \cdot \frac{P_{\text{stack}}}{P_{\text{seg}}} \text{ and } \sigma_{\text{stack}} = \sigma_{\text{seg}} \tag{20}$$

Physical properties of water and thermoelectric properties of the thermoelements are estimated by polynomial correlations [25].

3.2. Boundary conditions

The power output of the stack was set to $P_{\text{stack}} = 1\ \text{kW}_{\text{e}}$. The hot water inlet ($T_{\text{w,h,in}}$) and outlet ($T_{\text{w,h,out}}$) temperatures were varied in the range $T_{\text{w,h,in}} = 313$–413 K and $T_{\text{w,h,out}} = 303$–393 K, respectively, yielding hot water temperature differences ($\Delta T_{\text{w,h}}$) in the range $\Delta T_{\text{w,h}} = 10$–$110$ K. The cold water inlet ($T_{\text{w,c,in}}$) and outlet ($T_{\text{w,c,out}}$) temperatures were set to $T_{\text{w,c,in}} = 293$ K and $T_{\text{w,c,out}} = 298$ K, respectively, yielding the cold water temperature difference $\Delta T_{\text{w,c}} = 5$ K. The mass flow rates of hot ($m_{\text{stack,h}}$) and cold water ($m_{\text{stack,c}}$) were adjusted to satisfy the prescribed hot/cold water outlet temperatures. The axis of symmetry was set at the middle of the water channels (dashed–dotted line in Fig. 2). The pressure at the inlets to the channels is 5 bars.

3.3. Model parameters

The geometric parameters were ranging as follows:

(1) stack segment length $L = 300$–1500 mm, i.e., $N_{\text{array}} = 10$–50
(2) leg length $l = 0.5$–4 mm and
(3) hot/cold half-channel thicknesses $\{t_{\text{h}}, t_{\text{c}}\} = 0.1$–$1$ mm.

The model parameters are shown in Table 1.

3.4. Numerical solution

The coupled governing Eqs. (1)–(19) were implemented in a FORTRAN code and solved iteratively until the convergence criterion $|(T_{\text{w,h,i}}^{\gamma} - T_{\text{w,h,i}}^{\gamma-1})/T_{\text{w,h,i}}^{\gamma}| \leqslant 10^{-6}$ for all elements (i) and the overall energy balance $|(\Delta Q_{\text{h}} - \Delta Q_{\text{c}} - P_{\text{seg}})/\Delta Q_{\text{h}}| \leqslant 10^{-4}$ were satisfied, where $\Delta Q_{\text{h}} = m_{\text{seg,h}} \cdot c_{\text{p,w}} \cdot \Delta T_{\text{w,h}}$ and $\Delta Q_{\text{c}} = m_{\text{seg,c}} \cdot c_{\text{p,w}} \cdot \Delta T_{\text{w,c}}$.

3.5. Comparison with CFD-based model

The steady-state momentum and heat balance equations for the stack segment have been solved using computational fluid

Table 1
Model parameters.

Parameter	Value	Unit	Source
P_{stack}	1	kW	Set
$T_{\text{w,h,in}}$	313–413	K	Model parameter
$T_{\text{w,h,out}}$	303–393	K	Model parameter
A_{leg}	1.05×1.05	mm^2	Assumed
A_{plate}	30×30	mm^2	Assumed
l	0.5–4	mm	Model parameter
L	0.3–1.5	m	Model parameter
N_{array}	10–50	–	Model parameter
M	254	–	Set
t_{plate}	0.5	mm	Assumed
t_{Cu}	1	mm	Assumed
t_{c}	0.1–1	mm	Model parameter
t_{h}	0.1–1	mm	Model parameter
W	30	mm	Set
$\kappa_{p\text{-type}}$	1.13–1.36	W m^{-1} K^{-1}	Assumed [17]
$S_{p\text{-type}}$	204–235	μV K^{-1}	Assumed [17]
$\rho_{p\text{-type}}$	10.4–16.3	μΩ m	Assumed [17]
$\kappa_{n\text{-type}}$	1.26–1.38	W m^{-1} K^{-1}	Assumed [17]
$S_{n\text{-type}}$	−215 to −207	μV K^{-1}	Assumed [17]
$\rho_{n\text{-type}}$	11–15.5	μΩ m	Assumed [17]
$\hat{\rho}$	5e−9	Ω m^2	Assumed [27]

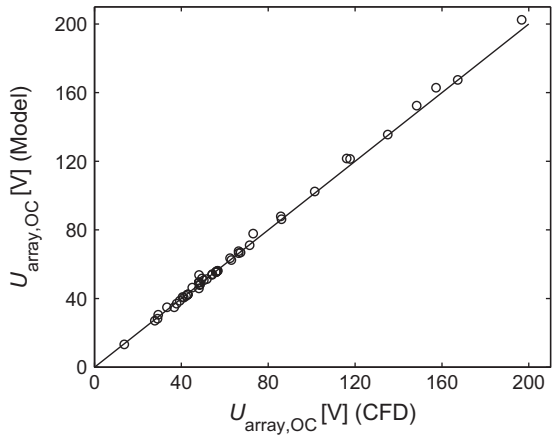

Fig. 3. Parity plot of the stack segment's open-circuit voltage $U_{array,OC}$ simulated by the heat transfer model and extracted from CFD. The coefficient of determination is $R^2 = 0.997$. The mean relative error is $\varepsilon = 3\%$.

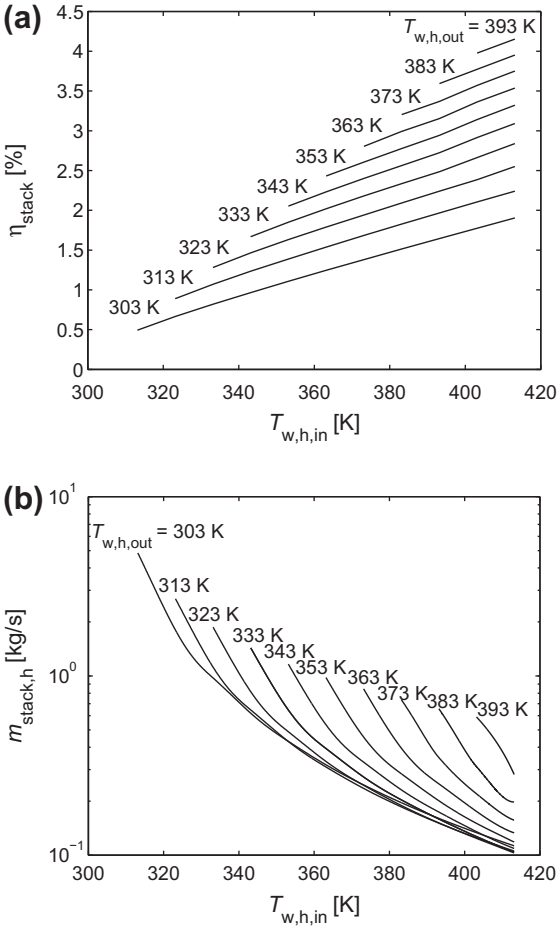

Fig. 4. (a) The heat-to-electricity efficiency and (b) the hot mass flow of the stack as function of the hot water inlet and outlet temperature for the case of maximized heat-to-electricity efficiency.

dynamics (CFD) software ANSYS CFX 13.0 [26] in order to obtain the rigorous temperature profiles of cold and hot sides of the legs along a segment. Open circuit voltages were then calculated using the mean temperature differences across the TEC modules and compared in Fig. 3 with those calculated based on the heat transfer model described in this work. The high coefficient of determination

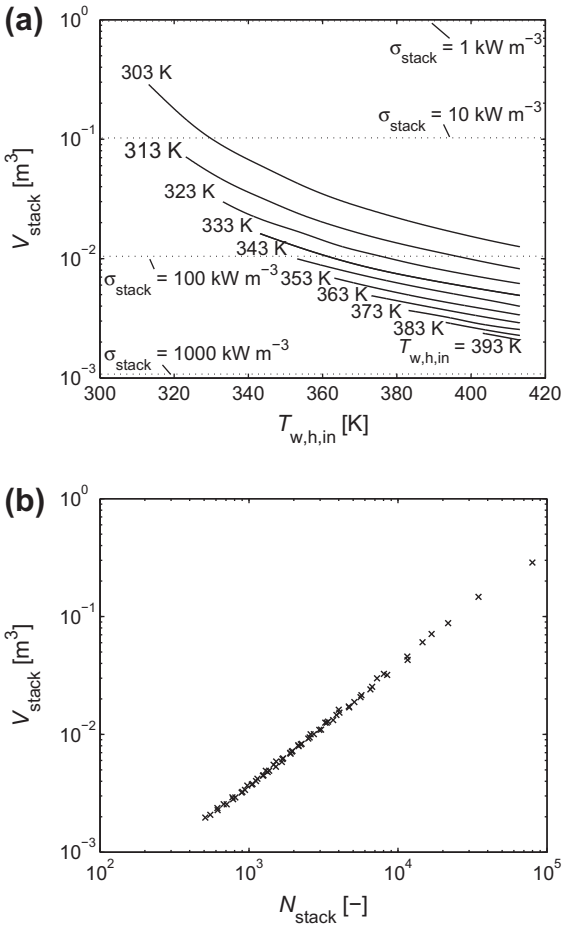

Fig. 5. (a) The stack volume and the power density as function of the hot water inlet and outlet temperature; and (b) the stack volume as function of the number of TEC modules in the stack for the case of minimized stack volume.

in this parity plot ($R^2 = 0.997$) implies good agreement between the two methods, further supported with mean relative error of $\varepsilon = 3\%$.

4. Simulations of a 1 kW_{el} stack

A stack delivering the useful power output $P_{stack} = 1\ kW_{el}$ has been optimized by varying geometric parameters at a given set of hot water inlet ($T_{w,h,in}$) and outlet ($T_{w,h,out}$) temperatures having either (a) maximum heat-to-electricity efficiency or (b) minimum size (maximum power density) as goal function.

4.1. Maximum heat-to-electricity efficiency

The heat-to-electricity efficiency (η_{stack}) as function of $T_{w,h,in}$ and $T_{w,h,out}$ is shown in Fig. 4a. It almost linearly increases with $T_{w,h,in}$ and $T_{w,h,out}$, implying a stronger dependency on the latter. The calculated values range from $\eta_{stack} = 0.5\%$, obtained for $T_{w,h,in} = 313$ K and $T_{w,h,out} = 303$ K; to $\eta_{stack} = 4.2\%$ for $T_{w,h,in} = 413$ K and $T_{w,h,out} = 393$ K.

Fig. 4b presents the effect of $T_{w,h,in}$ and $T_{w,h,out}$ on the hot water mass flow ($m_{stack,h}$). $m_{stack,h}$ monotonically decreases with $T_{w,h,in}$ but increases with $T_{w,h,out}$. The values range from $m_{stack,h} = 4.85$ kg/s, calculated for $T_{w,h,in} = 313$ K and $T_{w,h,out} = 303$ K, to $m_{stack,h} = 0.28$ kg/s, calculated with $T_{w,h,in} = 413$ K and $T_{w,h,out} = 303$ K. One should notice that increase in $T_{w,h,in}$ leads to an increase in η_{stack} but a decrease in $m_{stack,h}$ while both η_{stack} and $m_{stack,h}$ increase with an increase in $T_{w,h,out}$.

Table 2
Summarized results for maximized η_{stack} and minimized V_{stack} (maximized σ_{stack}).

		(a) Maximized η_{stack}			(b) Minimized V_{stack}			Comparing (a) to (b)	
$T_{w,h,out}$ (K)	$T_{w,h,in}$ (K)	η_{stack} (%)	V_{stack} (m^3)	σ_{stack} (kW m^{-3})	η_{stack} (%)	V_{stack} (m^3)	σ_{stack} (kW m^{-3})	$\eta_{stack,(a)}/\eta_{stack,(b)}$ (–)	$V_{stack,(a)}/V_{stack,(b)}$ ($\sigma_{stack,(b)}/\sigma_{stack,(a)}$) (–)
313	303	0.5	0.9075	1.1	0.16	0.2871	3.5	3.13	3.16
413	303	1.9	0.0611	16.4	0.78	0.0146	68.5	2.44	4.18
413	393	4.2	0.0135	74.1	2.1	0.0021	476.0	2.00	6.41

4.2. Minimum stack volume

The stack volume (V_{stack}) and the power density (σ_{stack}) are shown in Fig. 5a as function of $T_{w,h,in}$ and $T_{w,h,out}$. V_{stack} monotonically decreases and σ_{stack} monotonically increases with $T_{w,h,in}$ and $T_{w,h,out}$. The stack volumes range from $V_{stack} = 0.29\ m^3$ ($\sigma_{stack} = 3.5$ kW m^{-3}), calculated for $T_{w,h,in} = 313$ K and $T_{w,h,out} = 303$ K, to $V_{stack} = 0.0021\ m^3$ ($\sigma_{stack} = 476$ kW m^{-3}) obtained with $T_{w,h,in} = 413$ K and $T_{w,h,out} = 393$ K.

Fig. 5b is showing V_{stack} as function of the number of modules (N_{stack}) for all simulated hot inlet and outlet temperatures. The data points indicate a linear relationship (correlation factor of 0.9947). The number of modules ranges from $N_{stack} = 550$ to $N_{stack} = 79{,}740$ as calculated with $V_{stack} = 0.0021\ m^3$ and $V_{stack} = 0.29\ m^3$, respectively.

5. Summary and conclusions

A heat transfer model coupling 1D conduction through the thermoelement legs with convection to and from the legs has been implemented in order to investigate the performance of a thermoelectric stack as function of operating parameters and stack geometry. The simulated open-circuit voltages have been found to be within 3% mean relative error as compared to those calculated via CFD.

A stack delivering the useful power output $P_{stack} = 1\ kW_e$ has been optimized by varying geometric parameters at a given set of hot water inlet ($T_{w,h,in}$) and outlet ($T_{w,h,out}$) temperatures having as the goal function either (a) maximum efficiency or (b) minimum size (maximum power density). The key results are summarized in Table 2, implying strong dependency of both η_{stack} and V_{stack} (σ_{stack}) on $T_{w,h,in}$ and $T_{w,h,out}$.

The results have opened the possibility to perform economic analyses considering the costs of the TEC stack and the geothermal system in order to define the configuration and operating parameter range that are optimal from a commercial standpoint.

Appendix A

The magnitude of convective and radiative heat exchange between the hot and cold plates relative to the heat conducted through the thermoelement legs has been evaluated by CFD based on the following worst-case-scenario, chosen to overstate the contributions of convective and radiative transfers:

(1) Hot side temperature of 413 K (the maximum considered by simulations).
(2) Cold side temperature of 293 K (the minimum considered by simulations).
(3) Leg length of 4 mm (the longest considered by simulations).

The CFD model considers a 4-leg module. 2 *p*/*n*-type thermoelement leg pairs and the ambient air are simulated, as shown in Fig. A1. The thermoelement legs have dimensions of $4 \times 1.05 \times 1.05\ mm^3$ and a distance of 0.92 mm between neighboring legs. Both, the dimensions of the legs and the distance between neighboring legs correspond to those for the investigated 254-leg modules. The thermal resistance of the Al_2O_3 plates is neglected, i.e. they have no thickness, and constant temperature conditions are imposed on the hot ($T_h = 413$ K) and cold side ($T_c = 293$ K) of the thermoelement legs (indicated by solid lines). Symmetry boundaries are set at the lateral sides (indicated by dashed–dotted lines). Radiative heat exchange is simulated by the Monte Carlo method using 10^9 rays. The emissivities of the Al_2O_3 plates and thermoelement legs are 0.3 and 0.7, respectively. The CFD mesh contains 291,254 elements where the *p*/*n*-type thermoelement legs and the air domain have hexahedral and tetrahedral cells, respectively. Convergence was achieved when the residuals were $<10^{-6}$.

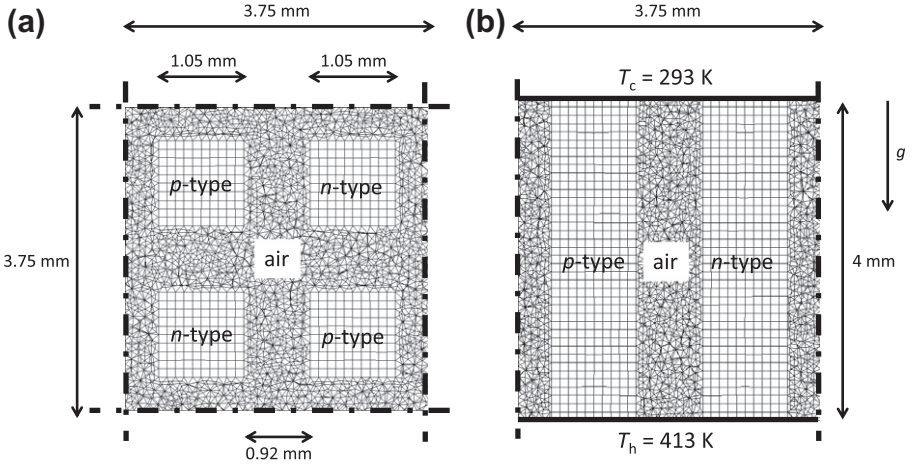

Fig. A1. (a) Cross-section and (b) longitudinal section of CFD model consisting of 2 *p*/*n*-type thermoelement leg pairs and air domain. Indicated are the dimensions, the temperature boundary conditions (solid lines), the symmetry boundaries (dashed dotted lines), and the gravitational force (g). The mesh contains 291,254 elements.

Table A1
Heat conduction, heat convection and radiative heat exchange in the 254-leg module.

	(W)	(%)
Heat conduction	11	95
Heat convection	0.5	4.2
Radiative heat exchange	0.1	0.8

The CFD results scaled to a 254-leg module are shown in Table A1.The estimated combined heat transfer by radiation and convection (0.6 W) has only a contribution of 5% to the total heat transfer (11.6 W).

References

[1] Geothermie Schweiz, January 2012. <http://www.geothermie.ch/>.
[2] Geothermie Deutschland, January 2012. <http://www.geothermie.de/>.
[3] Lund JW, Freeston DH, Boyd TL. Direct application of geothermal energy: 2005 Worldwide review. Geothermics 2005;34:691–727.
[4] Eisenhut C, Bitschi A. Thermoelectric conversion system based on geothermal and solar heat 25th international conference on thermoelectrics (ICT), 2006. Vienna, Austria; August 6–10, 2006. p. 510–5.
[5] Bitschi A. Modelling of thermoelectric devices for electric power generation. PhD thesis, ETH Zurich; 2009.
[6] Rowe DM. Review: thermoelectric waste heat recovery as a renewable energy source. Int J Innov Energy Syst Power 2006;1:13–23.
[7] Goldschmid HJ, Nolas GS. A review of the new thermoelectric materials. In: 20th International conference on thermoelectrics. Beijing, PR China; 2001.
[8] Min G. Thermoelectric module design theories. Thermoelectrics handbook: macro to nano. Boca Raton, USA: CRC Press; 2006.
[9] Rowe DM. General principles and basic considerations. Thermoelectrics handbook: macro to nano. Boca Raton, USA: CRC Press; 2006.
[10] Goldschmid HJ. Introduction to thermoelectricity. 1st ed. Berlin: Springer; 2009.
[11] Yamashita O, Sugihara S. High-performance bismuth-telluride compounds with highly stable thermoelectric figure of merit. J Mater Sci 2005;40: 6439–44.
[12] Yu J, Zhao H. A numerical model for thermoelectric generator with the parallel-plate heat exchanger. J Power Sources 2007;172:428–34.
[13] Esartea J, Minb G, Roweb DM. Modelling heat exchangers for thermoelectric generators. J Power Sources 2001;93:72–6.
[14] Crane DT, Jackson GS. Optimization of cross flow heat exchangers for thermoelectric waste heat recovery. Energy Convers Manage 2004;45: 1565–82.
[15] Bélanger S, Gosselin L. Thermoelectric generator sandwiched in a crossflow heat exchanger with optimal connectivity between modules. Energy Convers Manage 2011;52:2911–8.
[16] Bethancourt A, Echigo R, Yoshida H. Thermoelectric conversion analysis in a counter-flow heat exchanger. In: The thirteenth international conference on thermoelectrics; 1994. p. 299–304.
[17] Quick-Ohm, January 2012. <http://www.quick-ohm.de/bauteile.html>.
[18] Kundu PK, Cohen IM. Fluid mechanics. 4th ed. San Diego: Academic Press; 2007.
[19] Patankar S. Numerical heat transfer and fluid flow. New york, USA: Taylor & Francis; 1980.
[20] Bejan A. Convection heat transfer. 2nd ed. J. Wiley; 1995.
[21] Shah RK, London AL. Laminar flow forced convection in ducts. New York: Academic Press; 1978.
[22] Kakac S, Shah RK. Handbook of single-phase convective heat transfer. New York: Wiley & Sons; 1987.
[23] Gnielinski V. Ein neues Berechnungsverfahren für die Wärmeübertragung im Übergangsbereich zwischen laminarer und turbulenter Rohrströmung. Forsch Ingenieurwes 1995;61:240–8.
[24] Yamashita O. Effect of linear temperature dependence of thermoelectric properties on energy conversion efficiency. Energy Convers Manage 2008;49:3136–69.
[25] Properties DIfP. DIPPR Project 801 – Full Version: Design Institute for Physical Property Research/AIChE; 2010.
[26] ANSYS Inc., ANSYS CFX 13.0. 2011.
[27] Kuznetsov VL, Vedernikov MV. Thermocouple with a passive high temperature superconductor leg. Thermoelectrics handbook: macro to nano. Boca Raton, USA: CRC Press; 2006.